Desalination and Water Treatment
www.deswater.com

doi:10.5004/dwt.2017.20296

69 (2017) 344–351
March

Chemical desorption of non-condensable gases in horizontal-tube bundles for falling film evaporation

Luopeng Yang*, Yan Yang, Yang Liu, Shengqiang Shen

Key Laboratory of Ocean Energy Utilization and Energy Conservation, Ministry of Education, Dalian University of Technology, Dalian, 116024, China, Tel. +86 13130403891, Fax +86 411 84707963, email: yanglp@dlut.edu.cn (L. Yang), 1119743282@qq.com (Y. Yang), 741930488@qq.com (Y. Liu), zzbshen@dlut.edu.cn (S. Shen)

Received 21 June 2016; Accepted 24 October 2016

ABSTRACT

A reliable prediction of non-condensable gases (NCG) desorption is of great significance for enhancing heat transfer efficiency and optimizing the geometrical parameters in a horizontal-tube falling film evaporator. As chemical desorption of NCG in horizontal-tube falling film evaporation is a complex transfer process involving the coupling effects of fluid hydrodynamics, phase change and chemical reaction, little attention has been given to a predictive estimation of NCG desorption. A simulation model, which integrates the chemical reaction in seawater film with heat transfer of falling film evaporation, is developed to predict the carbon dioxide (CO_2) chemical desorption rate in horizontal-tube bundles. The size of differential volume elements in this model is determined by the controlling chemical reaction time rather than an assumption. The concentration of the carbonate system in the seawater film is calculated by the falling film evaporation rate which was predicted through modelling both external film evaporation and internal condensation. A good agreement between the predictions and the practical operating data of a multi-effect distillation (MED) desalination plant proves that the present model is reliable and accurate. The results show that the varying volume element sizes in tube bundles determined by chemical reaction time depend more on brine temperature than pH and salinity. The profiles of the concentration and pH in the brine film well explain the characteristics of the CO_2 chemical desorption rates in preheating and evaporation sections of tube bundles in a reference MED.

Keywords: CO_2 chemical reaction; Non-condensable gas; Horizontal-tube falling film evaporation; Volume element size

1. Introduction

Horizontal-tube falling film evaporation has been widely utilized in the thermal desalination industry by its advantages of high heat transfer efficiency, small temperature difference and thin liquid film. NCG desorption has received substantial attention due to its significance for enhancing thermal efficiency of falling film evaporators.

NCG have a seriously negative effect on condensing heat transfer rates and energy consumption. NCG, including carbon dioxide, oxygen and nitrogen, are released during falling film evaporation of seawater outside horizontal tubes. The accumulated NCG produce an extra heat and mass transfer resistance to prevent vapor from reaching tube wall and lower condensable partial pressure. As a result, even low concentration NCG severely deteriorates condensation heat transfer rates [1]. Since there is often neither a deaerator or a decarbonator in a MED desalination plant, it becomes highly vital to extract NCG from evaporators through adequate venting. For example, high pressure vapor, which is used to extract NCG by a thermal vapor

*Corresponding author.

Presented at the EDS conference on Desalination for the Environment: Clean Water and Energy, Rome, Italy, 22–26 May 2016.

compressor, accounts for 10% of the total consumed vapor in a MED desalination plant with a capacity of 12500 ton/day in China.

The NCG desorption in falling film evaporation includes physical and chemical desorption. Desorption of molecular gases of oxygen and nitrogen from seawater solution without chemical reactions is defined as physical desorption. When CO_2 is released by chemical reactions of carbonate species in seawater, this desorption is called chemical desorption. Since the theoretically maximum chemical desorption amount in a MED is ten times of physical desorption of oxygen and nitrogen [2], chemical desorption dominates the NCG desorption in falling film evaporators. Therefore, it is of great importance to predict the chemical desorption rates in order to improve the thermal efficiency of falling film evaporators.

A large amount of experimental and theoretical investigations on NCG have been performed. Due to the fact that chemical desorption, involving the combined effects of chemical reaction, phase change and fluid hydrodynamics, is a complex transfer process, most research [3-6] on NCG were focused on heat transfer mechanisms of condensation in presence of NCG and the effects of NCG on heat transfer performance of falling film evaporation. Little attention to NCG desorption process is paid even though accurately predicting NCG desorption rates is a prerequisite for these investigations. The first investigation on chemical desorption, based on simple reaction models and scarce data, were used to estimate NCG desorption rates by thermal desalination designers. As the effects of chemical reaction on the dissolved gas concentration and mass transfer rate enhancement were not taken into account, these predicted NCG desorption rates agreed with each other poorly. A theoretical model based on the coupling of mass transfer and chemical reaction kinetics were proposed to calculate CO_2 release in Multi-stage flashing (MSF) [7–8]. Since there exist key differences between seawater flashing and falling film evaporation in heat transfer machanism, hydrodynamics, operating temperatures and pressures, and flowing configurations, this model was further developed to calculate the CO_2 chemical desorption and carbonate concentrations in seawater film for falling film evaporation [9,10]. Although the accuracy of predicting CO_2 concentration in brine film depends on the size of volume elements in tube bundles, the size of the volume elements was roughly chosen to contain 3 tubes in this model in terms of researchers' experience. Temperatures and salinities of brine film on horizontal tube rows were assumed to linearly increase within the chosen elements in preheating and evaporation tube rows, separately. Thus, heat transfer calculation of falling film evaporation was not involved in this model.

The above mentioned deficiencies of chemical desorption simulation suggest that the existing model for CO_2 desorption rates can be improved by simulating profiles of temperature, salinity, and evaporation rate rather than assuming them. The volume element sizes should be determined by the chemical reaction time and calculated local velocities in brine film. A simulation model using a computer program of MATLAB, which integrates the chemical reaction desorption and heat transfer of falling film evaporation, is developed to predict the desorption rate of CO_2 in horizontal-tube bundles. The differential volume element in this model is the brine film volume flowing over tubes during the chemical reaction time. The CO_2 chemical desorption mechanism in fall film evaporation is obtained by analyzing profiles of carbonate species in brine film elements.

2. Numerical model formulation

2.1. Physical model

Seawater with a constant flow density of Γand a uniform temperature falls on the top of a horizontal tube at a height of H as show in Fig. 1. A liquid jet flows around both sides of the tube to form thin film under the combined effects of gravity, viscous force and surface tension, then converges at the bottom of the tube. Seawater film is heated to its saturated temperature at the liquid-vapor interface on the upper tube rows by the tube wall with a constant temperature. On the lower tube rows, part of brine film is evaporated by vapor condensation heat inside tubes. As falling film evaporation disturbs the chemical equilibrium in the carbonate system of seawater film, new CO_2 is continuously formed by the chemical reaction and released within brine film. Internal condensation is film-wise condensation as shown in Fig. 2. The condensate forms a continuous film covering the internal surface. The film flows over the surface under the actions of gravity and interfacial shear stress. The condensate flow pattern inside a tube is stratified as the condensate runs down the tube wall to form a layer at the bottom which is swept along the tube length by vapor flow.

Horizontal-tube falling film evaporation is modeled with the following assumptions:

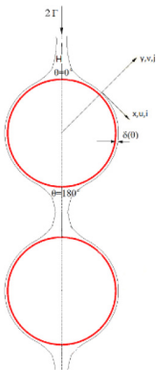

Fig. 1. Schematic of horizontal-tube falling film evaporation between adjacent tubes.

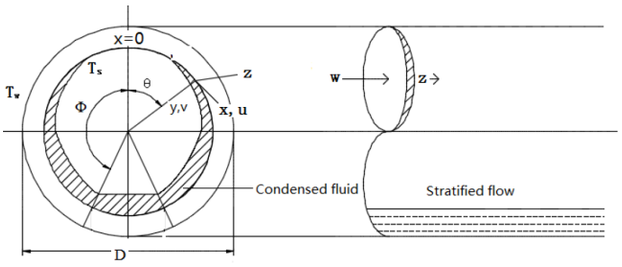

Fig. 2. Schematic of vapor condensation inside a horizontal tube.

(1) Seawater film flow outside a horizontal tube is either a laminar flow or a transition from laminar to slightly turbulent flow. Stratified two-phase flow occurs inside a horizontal tube.
(2) The curvature effect is neglected as film thickness of both seawater and condensate is small compared with the tube radius.
(3) Fluid properties within both seawater and condensate film remain constant because of small temperature differences in thin film.
(4) Liquid free falling on the top of a tube is the same as a jet impinging on a flat surface.
(5) Inter-facial waves and shear stresses at the liquid-vapor interface outside a tube are not taken into account.

2.2 Governing equations

The continuity, momentum and energy equations of external falling film evaporation in Fig. 1. are given as

$$\frac{\partial \mathrm{u}}{\partial \mathrm{x}}+\frac{\partial \mathrm{v}}{\partial \mathrm{y}}=0 \tag{1}$$

$$\mathrm{u}\frac{\partial u}{\partial x}+\mathrm{v}\frac{\partial v}{\partial y}=\mathrm{g}\sin(\mathrm{x}/R)+V\frac{\partial^2 U}{\partial Y^2} \tag{2}$$

$$\mathrm{u}\frac{\partial T}{\partial \mathrm{x}}+\mathrm{v}\frac{\partial T}{\partial \mathrm{y}}=\frac{\mathrm{k}}{\rho C_P}\frac{\partial^2 T}{\partial \mathrm{y}^2} \tag{3}$$

A starting velocity near the impinging point on the top of a tube is given as [11]

$$\mathrm{u}_0=C\times\left[\left(2\eta-3\eta^3+\eta^4\right)+\frac{\Lambda}{6}\left(\eta-3\eta^2+3\eta^3-\eta^4\right)\right] \tag{4}$$

$$\mathrm{v}_0=0 \tag{5}$$

where $\eta=\frac{\mathrm{y}}{\sigma_b}$

$$\sigma_b=\left(\frac{\Lambda\nu_f}{C}\right)^{0.5}$$

$$\Lambda=\left(\frac{\sigma_b}{\nu_f}\frac{\mathrm{du}}{\mathrm{dx}}\right)$$

$$C=0.787\frac{\rho g S}{\Gamma}$$

The boundary conditions are listed as
at $y = 0$, $x > 0$; $u = 0$, $v = 0$
at $y = \delta$, $x > 0$; + $\frac{\partial U}{\partial Y}=0$
at $y > 0$, $x = 0$; $u = u_o$, $v = v_o$
at $y = 0$, $x > 0$; $T = T_W$
at $y = \delta$, $x > 0$; $T = T_V$

Local heat transfer coefficient with in liquid film at an inclination angle of θ can be obtained as

$$h(\theta)=\frac{q}{T_W-T_V}=\frac{-K\left(\frac{\partial T}{\partial Y}\right)_{Y=0}}{T_W-T_V} \tag{6}$$

The continuity, momentum and energy equations at vapor-liquid interface of condensate inside a horizontal tube shown in Fig. 2 are given as

$$\dot{m}_i=\rho_l\left(v-u\frac{\partial\delta}{\partial x}-w\frac{\partial\delta}{\partial z}\right)_{y=\delta} \tag{7}$$

$$\left.\frac{\partial u}{\partial y}\right|_{y=\delta}=0 \tag{8}$$

$$\frac{\partial^2 w}{\partial y^2}=\frac{1}{\mu_l}\frac{dp}{dz})_f \tag{9}$$

$$(u\frac{\partial\delta}{\partial x}+w\frac{\partial\delta}{\partial z}-v)_{y=\delta}=\frac{k_l}{h_{fg}\rho_l}\frac{\partial T}{\partial y})_{y=\delta} \tag{10}$$

Film velocities in x-direction of u and in z-direction of velocity of w are givens as

$$u=g(\rho_l-\rho_v)(\delta y-0.5y^2)\sin\theta/\mu_l \tag{11}$$

$$w=\frac{c_1}{2}y^2+(\frac{\tau_i}{\mu_l}-\frac{1}{\mu_l}\frac{dp}{dz}\delta)y \tag{12}$$

Local temperature in liquid film is

$$T=T_w+(T_S+T_W)y/\delta \tag{13}$$

The boundary conditions of film velocity and temperature are
$u = w = 0$ $T = T_W$ at $y = 0$
$T = T_S$ and $y = \delta$
The equations for u, w, T and interfacial energy balance equation are substituted into continuity equation, thus a partial differential equation for film thickness is given as

$$\frac{\partial \mathrm{C_i}}{\partial t}=\mathrm{D_i}\left(\frac{\partial^2 \mathrm{C_i}}{\partial x^2}+\frac{\partial^2 \mathrm{C_i}}{\partial y^2}+\frac{\partial^2 \mathrm{C_i}}{\partial z^2}\right)-\mathrm{U_x}\frac{\partial \mathrm{C_i}}{\partial x}-\mathrm{U_y}\frac{\partial \mathrm{C_i}}{\partial y}$$
$$-\mathrm{U_z}\frac{\partial \mathrm{C_i}}{\partial z}+\mathrm{r_i} \tag{14}$$

Local heat transfer coefficient within liquid film at an inclination angle of θ and a distance from vapor inlet of z can be obtained as

$$h(\theta,z)=\frac{k_l}{\delta(\theta,z)} \tag{15}$$

The heat transfer processes of both falling film evaporation outside a horizontal tube and vapor condensate inside one are combined by the equivalent heat transfer rate. The detailed method of solution has been done by Xu [12].

2.3. Chemical desorption equations

A model, developed by H. Glade et al. [9,10], is used in this simulation to quantitatively describe the carbonate system in chemical equilibrium and chemical reaction kinetics and calculate the chemical desorption of CO_2 in a MED with horizontal tube falling film evaporation.

Among a number of chemical reactions which are involved by chemical desorption of CO_2, the rate-decisive reaction is:

$$CO_2 + OH^- \leftrightarrow HCO_3^- \tag{16}$$

A differential equation on the concentration field of component *i*, which considers molecular transport, convective transport and reaction, is

$$\frac{\partial C_i}{\partial t} = D_i\left(\frac{\partial^2 C_i}{\partial x^2} + \frac{\partial^2 C_i}{\partial y^2} + \frac{\partial^2 C_i}{\partial z^2}\right) - U_x\frac{\partial C_i}{\partial x} - U_y\frac{\partial C_i}{\partial y} - U_z\frac{\partial C_i}{\partial z} + r_i \tag{17}$$

The CO_2 desorption rate solution of the differential equations for Reaction (16) is

$$\dot{N}_{CO2} = k_L^0 A_{ph}\frac{(1+DK)\left(C_{CO2,B} - C_{CO2,ph}\right)}{1 + DK\dfrac{\tanh\left(Ha\sqrt{1+\dfrac{1}{DK}}\right)}{Ha\sqrt{1+\dfrac{1}{DK}}}} \tag{18}$$

Chemical reaction time of Reaction (16) is

$$t_R = \frac{1}{k_{OH^-}\left(\dfrac{K_W^{SW}}{K_1^{SW}} + \left[OH^-\right]\right)} \tag{19}$$

Film residence time is

$$t_1 = \sum\left(\partial\theta * d_o / 2 / U(\theta)\right) \tag{20}$$

$$t_2 = \sum\sqrt{(\partial z * 2 / g)} \tag{21}$$

The concentrations in the carbonate system are calculated based on the simulated evaporation rates. The temperature and salinity of brine film are predicted by the above combined models of external falling film evaporation and internal condensation. Thus, the CO_2 concentrations at the bulk and interface of film in Eq. (21) are calculated based on these simulation results.

2.4. Differential volume element size

For calculating the carbonate concentration and CO_2 chemical desorption in seawater film on horizontal tube bundles, differential volume element sizes are determined by the rules that controlling chemical reaction time equals to the residence time of seawater film. As local velocities in brine film along a horizontal tube are obtained by simulating falling film evaporation, the differential volume element sizes are brine film volumes flowing over the tubes during the chemical reaction time as shown in Fig. 3.

3. Results and discussion

3.1. Simulation model verification

Numerical results of local heat transfer coefficients for external falling film evaporation and internal condensation are compared with experimental data of Liu [13] and Shen [14] in Fig. 4. The comparison shows that the simulating predictions are in a good agreement with the data. An overestimation of external falling film heat transfer coefficients near the upper part of the tube is due to the uncertainty of the measuring data in the upper impinging region.

The predicted CO_2 chemical desorption is compared with the calculated result of H. Glade in a MED with five-effect evaporators [11] in Fig. 5. The comparison shows that the predictions are slightly underestimated, and that the difference of specific desorption rates increases from the first effect evaporator to the last one. The underestimation can be attributed to the volume element size. The element, which was artificially assumed to contain 3 tubes [15] by H. Glade, are calculated according to the chemical reaction time in seawater film in this paper. It's found in Table 1 that the calculated element numbers in five evaporators are evidently greater than the assumed ones. Specific CO_2 desorption rates decrease from the upper tubes to the bottom due to decreasing mass transfer coefficients and total inorganic carbon contents. The decreasing chemical desorption rates, together with the increasing element numbers, result in this overestimation.

Calculated evaporation temperatures in evaporators for a reference MED desalination plant are compared with

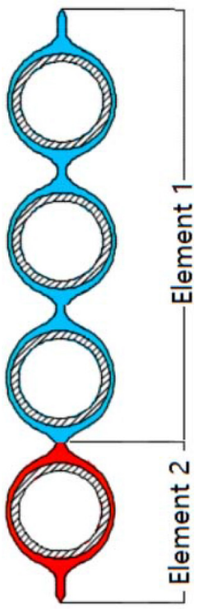

Fig. 3. Differential volume element size.

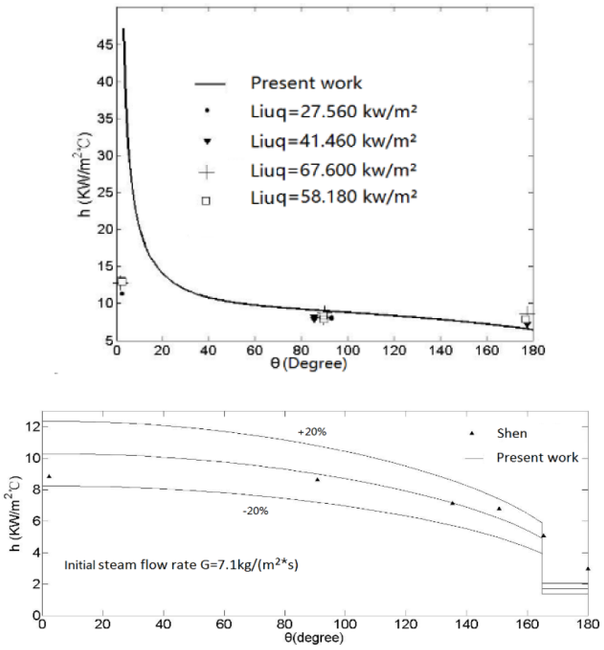

Fig. 4. Comparison of local heat transfer coefficients.

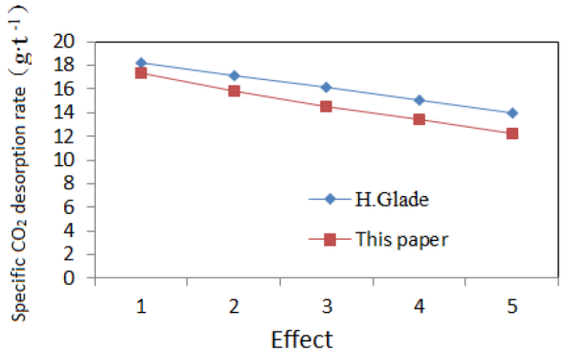

Fig. 5. Comparison of specific CO_2 desorption rates.

Table 1
Comparison of the volume element numbers

	H. Glade	This paper
Effect 1	35	101
Effect 2	35	100
Effect 3	35	99
Effect 4	35	91
Effect 5	35	74

practical data of t_3 in Table 2. The calculated ones include evaporation temperature, t_1, for evaporation without NCG and evaporation temperature, t_2, for evaporation in presence of NCG. The configuration and dimensions of the reference MED are presented in Fig. 6. and Table 3. Table 2 indicates that t_2 is close to t_3. The difference between t_1 and t_3 increases from the first effect to the last one due to increasing NCG accumulation. Compared with the overall heat transfer temperature difference of 2.6°C between internal vapor condensation and external falling film evaporation in the last evaporator, the temperature difference of 0.34°C between t_1 and t_3 is distinct. This proves that the negative effect of NCG on heat transfer rates is remarkable. A good agreement between t_2 and t_3 indirectly verifies the accuracy and reliability of the developed model of CO_2 desorption.

3.2 Chemical reaction time

Chemical reaction time with respect to brine temperature, pH and salinity in an evaporator, where inlet seawater at 42.6°C is preheated to its saturated temperature of 65°C, is presented in Fig. 7. The chemical reaction time apparently decreases with increasing brine temperature, pH and salinity. For the upper tubes in an evaporator where seawater is preheated to its saturated temperature and the salinity remains constant, a significant decrease in chemical reaction time results in a decrease in volume elements from 5 tubes to 1 tube. For the rest tubes where evaporation occurs, the chemical reaction time changes very smoothly with an increase in salinity and pH due to the fact that external falling film evaporation rates stay almost constant. As a result, the volume sizes in these tubes keep at the magnitude of 1 tube. Therefore, the brine temperature is the predominant effect on the chemical reaction time and the element size. As a decrease in evaporation rates with decreasing brine saturated temperature in an evaporator causes a large change in carbonate concentrations of brine film, a notable variation in chemical reaction time from the first effect evaporator to the last one results in a decrease in volume element sizes.

3.3 Carbonate concentration effect on desorption rates

Concentration profiles of CO_2, HCO_3^-, CO_3^{2-} and pH in brine film elements of the reference MED in Fig. 6 are presented in Fig. 8. As the pH decreases and the HCO^{3-} concentration increases in the preheating volume elements, the CO_2 concentration in the brine bulk increases according to the rate-decisive reaction of CO_2 chemical desorption, $CO_2 + OH^- \leftrightarrow HCO_3^-$ [11]. The CO_2 concentration at the liquid-vapor interface in brine film decreases due to a decrease in CO_2 solubility of brine film with increasing brine temperature. Thus, the increasing CO_2 concentration difference

Table 2
Comparison of evaporation temperatures

Evaporation temperatures (°C)	Effect 1	Effect 2	Effect 3	Effect 4	Effect 5	Effect 6
Calculated values without NCG t_1	61.61	58.42	55.31	52.33	49.31	46.14
This paper t_2	61.59	58.40	55.28	52.28	49.26	46.06
Practical values t_3	61.6	58.4	55.2	52.1	49.1	45.8

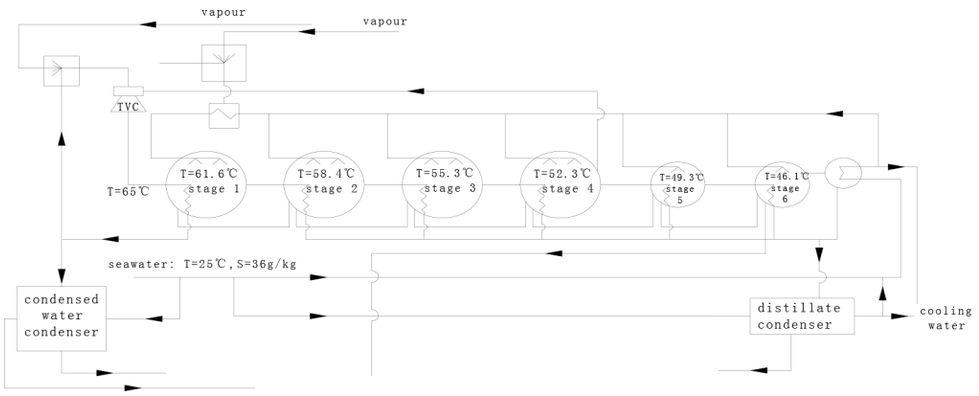

Fig. 6. Schematic of a reference MED process configuration.

Table 3
Dimensions of the reference MED

Dimension	Effect 1–4	Effect 5–6
Length of tubes, m	9.65	6.0
Tube outside diameter, m	0.0254	0.0254
Tube inside diameter, m	0.024	0.024
Number of tubes, m	13260	7611

between the bulk and liquid-vapor interface contributes to increasing CO_2 chemical desorption rates.

For evaporation volume elements, the chemical desorption, which is caused by evaporation disturbing the equilibrium in brine carbonate, results in an increase in pH and a decrease in HCO_3^- concentrations. In terms of $CO_2 + OH^- \leftrightarrow HCO_3^-$, the reducing driving force for CO_2 desorption leads to decreasing chemical desorption rates. Meanwhile, brine evaporation increases the concentrations of the. The opposite effects of chemical desorption and evaporation on the carbonate species concentrations are clearly shown in Fig. 8(b) where the concentration of HCO_3^- decreases at a lower speed with increasing volume element numbers. Thus evaporation partially compensates the decreasing chemical desorption rates.

4. Conclusions

Numerical simulations of chemical desorption of NCG in horizontal-tube bundles for falling film evaporation have been performed to gain deep insights into the chemical desorption mechanism. The differential volume element sizes in this model are chosen based on the chemical reaction time and simulated local velocities in brine film. The good agreement between the predictions and the experimental data validates the accuracy of the developed numerical model. The varying volume element sizes in tube bundles determined by chemical reaction time depend more on brine temperature than pH and salinity. The profiles of the concentrations and pH in brine film elements well explains the characteristics of the chemical desorption rates of CO_2 in preheating and evaporation sections of tube bundles in the reference MED.

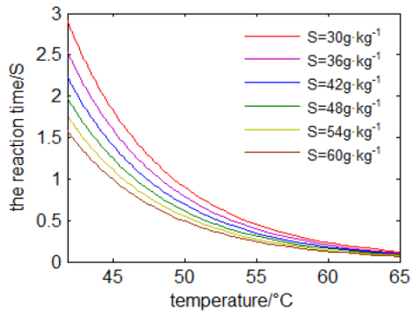

(a) pH = 7.7

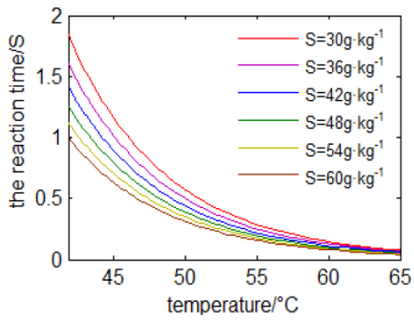

(b) pH = 7.9

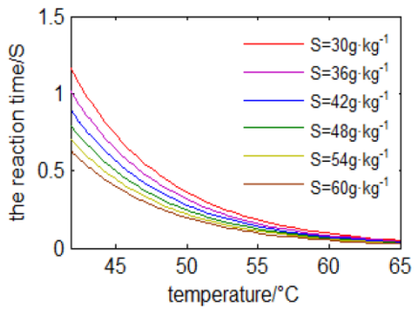

(c) pH = 8.1

Fig. 7. Chemical reaction time as a function of temperature, salinity and pH of brine film.

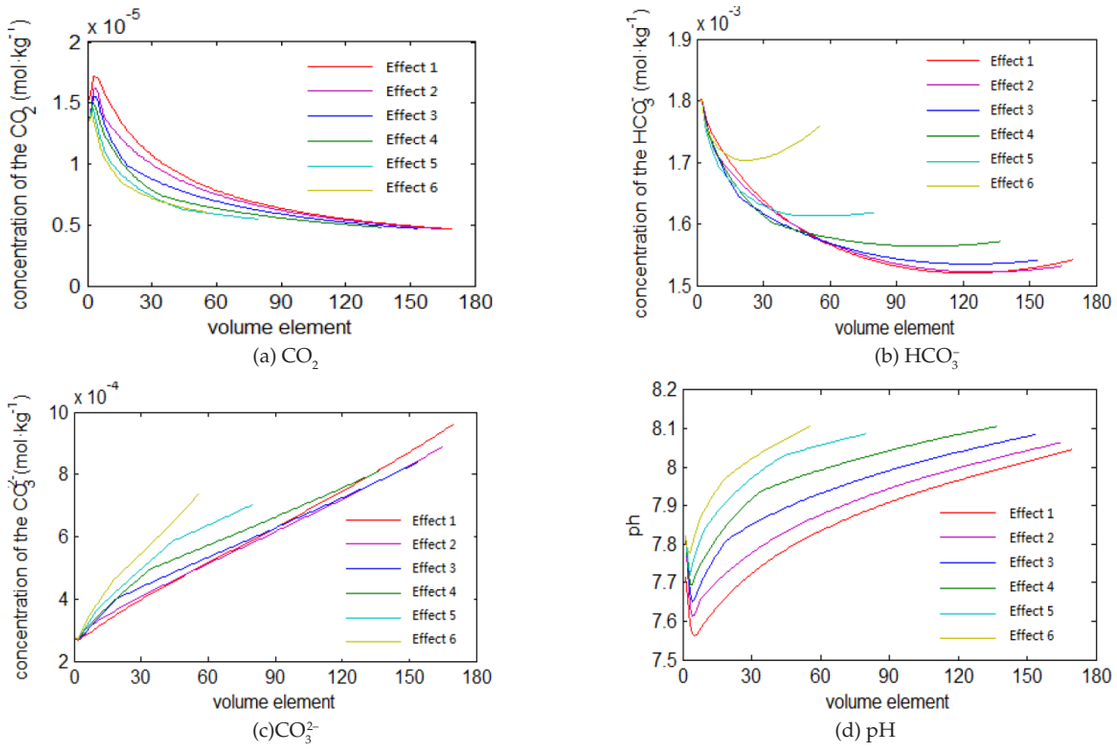

Fig. 8. Profiles of calculated carbonate concentrations in brine film elements of the reference MED.

Acknowledgement

This work was supported by "the National Natural Science Foundation of China (Grant No. 51576028).

Symbols

C	—	Species concentration
C_p	—	Specific heat at constant pressure, J/kg K
d	—	Diameter
D	—	Diffusivity
g	—	Gravitational acceleration, m/s^2
h	—	Convection heat transfer coefficient, W/m^2 K
Ha	—	Ha number
k	—	Thermal conductivity, W/m K
p	—	Pressure, Pa
Re	—	Reynolds number
T	—	Wall temperature, K or ˚C
t	—	Flow time, s
t_R	—	Response time
U	—	Velocity profile
u	—	Velocity in x-direction, m/s
u_o	—	Initial velocity
v	—	Velocity in y-direction, m/s
w	—	Velocity in z-direction, m/s
x	—	Horizontal coordinate
y	—	Vertical coordinate
z	—	Axial direction

Greek

δ	—	Film thickness, mm
θ	—	Stratified angle °
λ	—	Thermal conductivity, W/m K
μ	—	Dynamic viscosity, kg/m s
ρ	—	Density, kg/m^3
Γ	—	Flow density, kg/m s

Subscripts

fg	—	Phase change
l	—	Liquid phase
o	—	Extine
s	—	Saturation
SW	—	Seawater
v	—	Gas phase
w	—	Wall
W	—	Water

References

[1] R. Semiat, Y. Galperin, Effect of non-condensable gases on heat transfer in the tower MED seawater desalination plant, Desalination, 140 (2001) 27–46.
[2] H.E. Homig, Seawater and seawater distillation. Vulkan-Verlag Essen, 1978.
[3] M.K. Groff, S.J. Ormiston, H.M. Soliman, Numerical solution of film condensation from turbulent flow of vapor-gas mixtures in vertical tubes, Int. J. Heat Mass Transfer., 50 (2007) 3899–3912.
[4] S. Oh, S.T. Revankar, Experimental and theoretical investigation of film condensation with non-condensable gas, Int. J. Heat Mass Transfer., 49 (2006) 2523–2534.
[5] S. Oh, S.T. Revallkar, Effect of non-condensable gas in a vertical tube condenser, Nucl. Eng. Design., 235(16) (2005) 1699–1712.
[6] V. Dharma Rao, V. Murali Krishna, K.V. Sharma, P.V.J. Mohana Rao, Convective condensation of vapor in the presence of a non-condensable gas of high concentration in laminar flow in a vertical pipe, Int. J. Heat . Mass Transfer., 51 (2008) 6090–6101.

[7] H. Glade, Chemical reaction kinetics and mass transfer phenomena controlling the release of CO_2 in MSF distillers. Proc. IDA World Congress on Desalination and Water Reuse, San Diego, USA, 1999 375–388.
[8] H. Glade, K. Genthner, The carbonate system in MSF distillers, Proc. IDA World Congress on Desalination and Water Reuse, Bahrain, 2002.
[9] A.E. A1-Rawajfeh, H. Glade J. Ulrich, CO_2 release in multiple-effect distillers controlled by mass transfer with chemical reaction, Desalination, 156 (2003) 109–123.
[10] H. Glade, A.E. Al-Rawajfeh, Modeling of CO_2 release and the carbonate system in multiple-effect distillers, Desalination, 222 (2008) 605–625.
[11] N.A. Malamataris, V. Balakotaiah, Flow structure underneath the large amplitude waves of a vertically falling film, AICHE J. 54 (2008) 1725–1740.
[12] X Zhe-xuan, The numerical simulation of falling film evaporator on horizontal tubes, Master Thesis, Dalian University of Technology, June Dalian, (2013).
[13] P. Liu, The evaporating falling-film on horizontal tube, Ph.D. Thesis, University of Wisconsin-Madison, Wisconsin, August (1975).
[14] R. Liu, S.-Q. Shen, X.-H. Liu, L.-Y. Gong, Horizontal tube stratified condensate wet angle and circular heat exchange, Thermal Sci. Technol., 13(1) (2014) 10–14.
[15] A.E. Al-Rawajfeh, H. Glade, H.M. Qiblawey, J. Ulrich, Simulation of CO_2 release in multiple-effect distillers, Desalination, 166 (2004) 41–52.